QUANTUM INFORMATION


10.1126/sciadv.1500672

# Robust bidirectional links for photonic quantum networks

Jin-Shi Xu,[1,2]* Man-Hong Yung,[3,4,5]* Xiao-Ye Xu,[1,2] Jian-Shun Tang,[1,2] Chuan-Feng Li,[1,2]† Guang-Can Guo[1,2]

**Optical fibers are widely used as one of the main tools for transmitting not only classical but also quantum information. We propose and report an experimental realization of a promising method for creating robust bidirectional quantum communication links through paired optical polarization-maintaining fibers. Many limitations of existing protocols can be avoided with the proposed method. In particular, the path and polarization degrees of freedom are combined to deterministically create a photonic decoherence-free subspace without the need for any ancillary photon. This method is input state–independent, robust against dephasing noise, postselection-free, and applicable bidirectionally. To rigorously quantify the amount of quantum information transferred, the optical fibers are analyzed with the tools developed in quantum communication theory. These results not only suggest a practical means for protecting quantum information sent through optical quantum networks but also potentially provide a new physical platform for enriching the structure of the quantum communication theory.**

## INTRODUCTION

Photonic quantum technologies have developed rapidly in recent years and have shown promise for many applications in quantum information processing (QIP) such as quantum computing (*1*), quantum simulation (*2*), and quantum metrology (*3*). To scale up these applications, robust quantum communication links for short to medium distances (for example, 100 m or less) are required to be connected to different optical QIP modules. There, the problem of photon loss in optical fibers is negligible for the length scales considered (*4*); we can therefore ignore this problem for the purpose of building links for a quantum network (Fig. 1).

The decoherence problem of (polarization-encoded) photonic qubits can be divided into two parts, namely, the rotation of polarization (ambiguity of reference frame) and the dephasing of the relative phases between polarizations. The decoherence problem can be reduced to the dephasing problem only (that is, without basis rotation) with the use of PM fibers (*5*). This work is focused on turning these dephasing channels of PM fibers into robust links for quantum communication.

To deal with the dephasing problem, we can use one of the most well-known methods for protecting quantum information—quantum error correction (*6*), where logical qubits are encoded in many physical qubits. The approach has been realized experimentally (*7*). However, the resources required for encoding, decoding, and error detection remain technologically demanding.

Alternatively, another means to achieving robust quantum communication is through the use of decoherence-free subspace (DFS) (*8*–*29*), which is applicable when quantum states are beset with correlated errors. Despite its elegance, the current DFS approach for optical communications suffers from drawbacks, which make it challenging to achieve large-scale applications.

First, there remains a high demand for resources that are necessary to obtain deterministic entangled photons or to carry out entangling operations (with low efficiency) for the current quantum-optics technology (*30*). In particular, the encoding operation can be achieved with

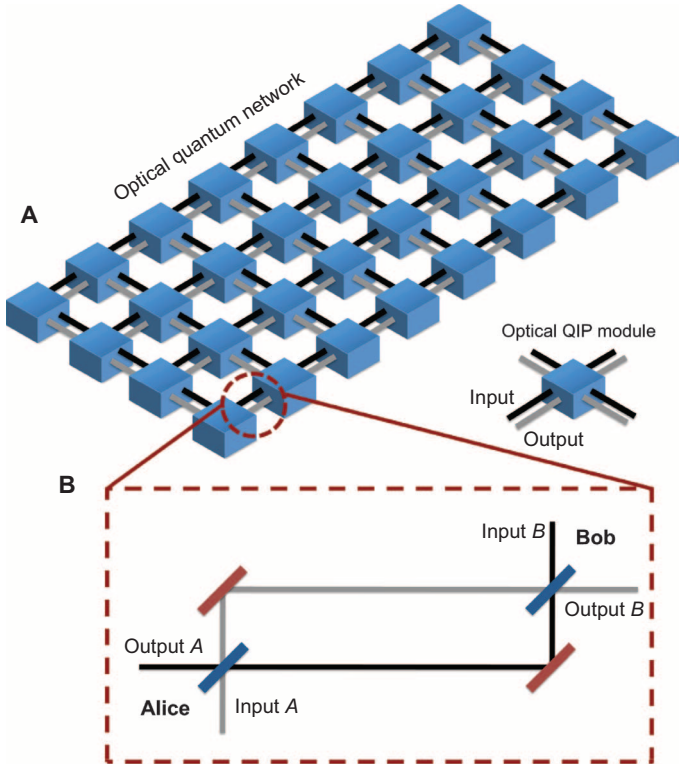


**Fig. 1. Optical quantum network.** (**A**) A quantum network where each QIP module is connected to other modules through an input port and an output port. (**B**) These input/output links can be constructed with our method using polarization-maintaining (PM) fibers. Here, we show the links that can transfer single qubits. To send entangled states of multiple qubits, we can either include more such transmission links or send through the same link sequentially.

[1]Key Laboratory of Quantum Information, University of Science and Technology of China, CAS, Hefei 230026, People's Republic of China. [2]Synergetic Innovation Center of Quantum Information and Quantum Physics, University of Science and Technology of China, Hefei, Anhui 230026, People's Republic of China. [3]Department of Physics, South University of Science and Technology of China, Shenzhen 518055, People's Republic of China. [4]Center for Quantum Information, Institute for Interdisciplinary Information Sciences, Tsinghua University, Beijing 10084, People's Republic of China. [5]Department of Chemistry and Chemical Biology, Harvard University, Cambridge, MA 02138, USA.
*These authors contributed equally to this work.
†Corresponding author. E-mail: cfli@ustc.edu.cn

the construction of the CNOT gate (*31*, *32*), but it requires a large number of ancillary photons during implementation (*33*).

Second, for the direct transfer of quantum states, most optical implementations of DFS (*23*, *25*) produce correct output states only probabilistically (that is, after selection), which limits the potential applicability of the methods for multiple uses.

Third, existing approaches (*18*, *19*, *23*, *25*, *28*, *29*) for quantum communication through fiber optics are unidirectional (that is, one-way communication) (*34*), which limits the range of their applications for quantum networks that would require frequent short-distance quantum communications.

To avoid the drawbacks of the previous DFS methods, we propose and experimentally realize an alternative approach to constructing robust quantum communication links that represent a simple and promising way of protecting quantum information through noisy optical fibers. Essentially, our setup involves a pair of optical fibers. The reason for using a pair of fibers instead of a single fiber is to eliminate the need for further additional active control, which is much more complicated in terms of implementation (see the Supplementary Materials for more details).

## RESULTS

### Experimental setup and the underlying design principle

Our experimental setup is shown in Fig. 2A. The key ingredients in our setup include a pair of optical PM fibers and a set of half-wave plates (HWPs). The two fibers are bundled together to maximize error correlation, as shown in Fig. 2B. In the experiment, we used polarization beam splitters (PBS) to encode and decode two PM fibers with the basis setting at the horizontal and vertical directions ($\{|H\rangle, |V\rangle\}$). The PBS behaves like a CNOT gate, with the path degrees of freedom (DOF) $\{|0\rangle, |1\rangle\}$ controlled by the polarization, where $|0\rangle$ and $|1\rangle$ represent the transmission and reflection cases, respectively. Different types of HWP setting in the interferometer allow our setup to be operated in either the bidirectional mode or the unidirectional mode. Here, we would focus on bidirectional use, where the angles of HWPs in the reflection path are set to 0° and those of HWPs in the transmission path are set to 45°. The case for the unidirectional mode (all HWPs in the interferometer are set to be 22.5°) is shown in the Supplementary Materials.

When the quantum state $|\phi_{in}\rangle = \alpha|H\rangle + \beta|V\rangle$ ($\alpha$ and $\beta$ are some unknown complex numbers and $|\alpha|^2 + |\beta|^2 = 1$) is sent from the *A* side to the *B* side (from left to right), the PBS entangles the path DOF, and the state becomes $|\phi_{ph}\rangle = \alpha|H\rangle|0\rangle + \beta|V\rangle|1\rangle$. The horizontal polarization along the transmitted path ($|0\rangle$) is unchanged, but the vertical polarization at the reflected path ($|1\rangle$) flips to the horizontal state. The information of the input quantum state is then transferred to the path DOF, $|\phi_{ph}\rangle = |H\rangle(\alpha|0\rangle + \beta||1\rangle)$. After the photon passes through the pair of PM fibers, phase shifts $\tau_{H0,H1}(\omega)$ are induced from each path for each frequency component $\omega$, $|\phi_{ph}\rangle = |H\rangle(\alpha e^{i\tau_{H0}(\omega)}|0\rangle + \beta e^{i\tau_{H1}(\omega)}||1\rangle)$. Then, the HWP at the reflected path flips the polarization back to $|V\rangle$, which gives the following state: $|\phi_{ph}\rangle = \alpha e^{i\tau_{H0}(\omega)}|H\rangle|0\rangle + \beta e^{i\tau_{H1}(\omega)}|V\rangle||1\rangle$.

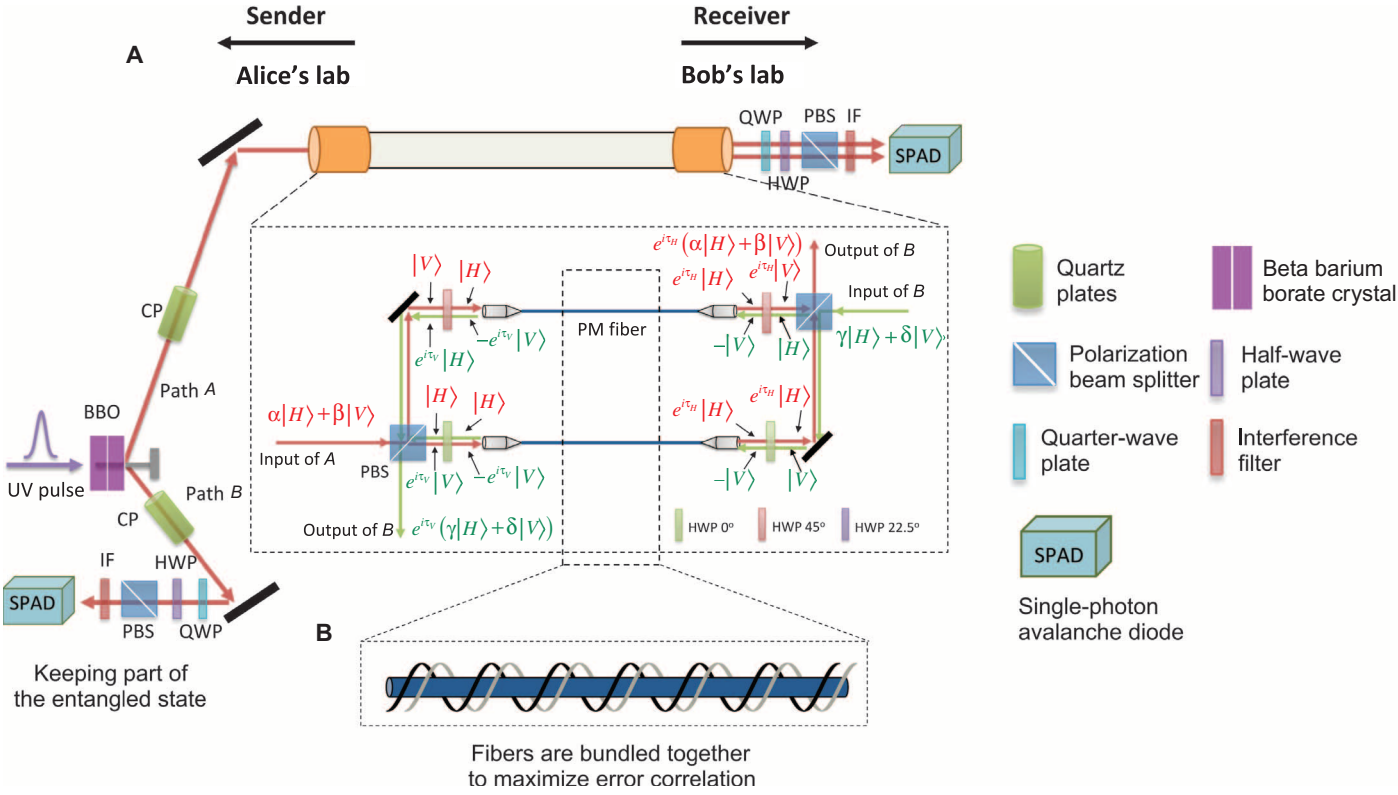


**Fig. 2. Experimental setup.** (**A**) The full setup for entanglement distribution over a pair of 120-m-long PM fibers. Part of the entangled photon is kept by Alice's laboratory; another part of the entangled pair enters the interferometric unit. The photons are finally detected by single-photon avalanche detectors (SPADs) with 3-nm interference filters (IFs) in front of them. (**B**) The two fibers are bundled together to maximize error correlation.

Finally, the two paths cross at the decoding PBS, which separates the path DOF, $|\phi_{ph}\rangle = (\alpha e^{i\tau_{H0}(\omega)}|H\rangle + \beta e^{i\tau_{H1}(\omega)}|V\rangle)|0\rangle$. The corresponding reduced density matrix of the polarization state has the following form

$$\begin{pmatrix} |\alpha|^2 & \alpha\beta^* e^{i\Delta\tau_H} \\ \alpha^*\beta e^{-i\Delta\tau_H} & |\beta|^2 \end{pmatrix} \quad (1)$$

with $\Delta\tau_H = \tau_{H0} - \tau_{H1}$. Whenever the errors are highly correlated, that is, $\tau_{H0} \approx \tau_{H1} \equiv \tau_H$, the signal photon with a state identical to the initial one can be detected along the path $|0\rangle$. The phase difference $\Delta\tau_H$ causes dephasing to the output state as expected.

In a similar but not identical way, quantum information can be sent from the *B* side to the *A* side (from right to left). As shown in Fig. 2A, for an input general photon state $|\psi_{in}\rangle = \gamma|H\rangle + \delta|V\rangle$ ($\gamma$ and $\delta$ are some unknown complex numbers and $|\gamma|^2 + |\delta|^2 = 1$) at the *B* side, the corresponding reduced density matrix of the output state at the *A* side has the following form

$$\begin{pmatrix} |\gamma|^2 & \gamma\delta^* e^{i\Delta\tau_V} \\ \gamma^*\delta e^{-i\Delta\tau_V} & |\delta|^2 \end{pmatrix} \quad (2)$$

with $\Delta\tau_V = \tau_{V0} - \tau_{V1}$ ($\tau_{V0}$ and $\tau_{V1}$ represent the obtained phases when the photon passes through paths $|0\rangle$ and $|1\rangle$, respectively). Whenever the errors are correlated, that is, $\tau_{V0} \approx \tau_{V1} \equiv \tau$, the signal photon with a state identical to the initial one can be detected along the path $|0\rangle$ and the phase difference $\Delta\tau_V$ causes dephasing to the output state as expected.

## Coherent information of noisy quantum channels

To quantify the amount of quantum information that can be transmitted through our setup, we analyzed the data through the tools developed in quantum communication theory, instead of just measuring the fidelity of output states. However, as far as we are aware, the parameterization in this work is not widely known; therefore, we provide a concise but self-contained theoretical background below.

Quantitatively, the amount of quantum information transmitted through a noisy channel (Fig. 3) can be quantified by coherent information (*35*), $\mathcal{I}_c = S[\mathcal{E}(\rho_A)] - S[(\mathcal{E} \otimes I)(|\Psi\rangle_{AB}\langle\Psi|)]$, where $\mathcal{E}$ represents the quantum operation of a noisy channel, $\rho_A$ is the initial input state, and $|\Psi\rangle_{AB}$ is the purified state of $\rho_A$; that is, $\rho_A = \mathrm{Tr}_B(|\Psi\rangle_{AB}\langle\Psi|)$. $I$ is the identity operator, and $S[\rho] = -\mathrm{Tr}\,(\rho \log \rho)$ is the von Neumann entropy of a density matrix $\rho$. Here, the term "channel" is equally applicable to either a single fiber or the combined fibers in the experimental setup. The quantum capacity

$$\mathcal{Q}_1 \equiv \max_{\rho} \mathcal{I}_c \quad (3)$$

of a single-use quantum channel is defined by the maximal coherent information that can be achieved over all possible input states $\rho$. More generally, quantum capacity is defined through the average coherent information transmitted through multiple uses (*36*–*38*); but for dephasing channels (*39*), both definitions are equivalent.

For any state $\rho$ in the two-dimensional space, it can always be expressed in some orthogonal basis $\{|\psi\rangle, |\psi_\perp\rangle\}$ as $\rho = \lambda_0|\psi\rangle\langle\psi| + \lambda_1|\psi_\perp\rangle\langle\psi_\perp|$, where $|\psi\rangle = \cos\theta\,|0\rangle + \sin\theta\, e^{i\phi}|1\rangle$ and $|\psi_\perp\rangle = \sin\theta\,|0\rangle - \cos\theta\, e^{i\phi}\,|1\rangle$, and $\lambda_0 + \lambda_1 = 1$. The corresponding purified state can be written as $|\Psi\rangle = \sqrt{\lambda_0}|\psi\rangle|0\rangle + \sqrt{\lambda_1}|\psi_\perp\rangle|1\rangle$. Therefore, the coherent information $\mathcal{I}_c$ for any quantum channel transmitting qubits depends only on three independent parameters, namely, $\lambda_0$, $\theta$, and $\phi$, which are used to describe the experimental data.

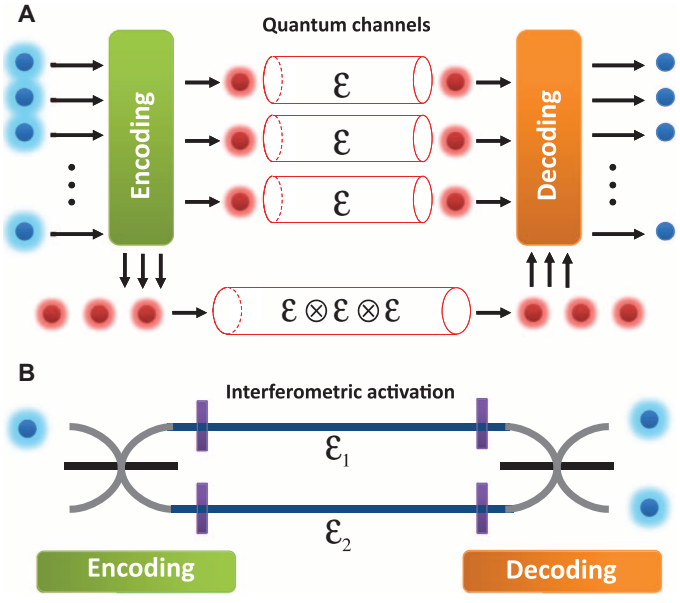


**Fig. 3. Quantum information transmission through noisy channels.** (**A**) In the standard quantum channel theory, where channels are assumed to be independent and uncorrelated, photons can pass through each channel or the same channel one after another, following a tensorial decomposition. (**B**) In the setting of interferometric activation over optical fibers, a photon, carrying a qubit of information in the polarization basis, can travel through different channels, inducing an extra DOF to compensate for correlated noise through interference.

To fully characterize the action of a channel on the input signals $\rho$, we experimentally performed a full quantum process tomography (*40*, *41*) on the quantum channels. By expanding the output state $\mathcal{E}(\rho)$ with a complete set of basis $\hat{E}_m$ of the Pauli operators $\{I, X, Y, Z\}$, the operation of the quantum process can be expressed as $\mathcal{E}(\rho) = \sum_{mn}\chi_{mn}\hat{E}_m\rho\hat{E}_n^\dagger$. In this representation, the $4 \times 4$ matrix $\chi$ completely and uniquely characterizes the physical process $\mathcal{E}$. The matrix elements $\chi_{mn}$' can be constructed from experimental tomographic measurements (*42*) of four input signals, namely, $\left\{|H\rangle, |V\rangle, |D\rangle \equiv \frac{1}{\sqrt{2}}(|H\rangle + |V\rangle), |R\rangle \equiv \frac{1}{\sqrt{2}}(|H\rangle - i|V\rangle)\right\}$.

## Main experimental results for single-fiber characterization

Figure 4 (A to D) shows the experimental results for single-fiber characterization. Figure 4A shows the experimental real part of the $\chi$ matrix, denoted as $\chi^{(s)}$, of the single PM fiber (the corresponding imaginary part is small and is shown in the Supplementary Materials). Note that the two nearly equal distributions of $I$ and $X$ indicate the strong dephasing effect of the fiber on the basis of $|D\rangle$ and $|J\rangle$ ($\equiv \frac{1}{\sqrt{2}}(|H\rangle - |V\rangle)$); that is, $\mathcal{E}(\rho) \approx (I\rho I + X\rho X)/2 \equiv \chi^{(i)}(\rho)$. The fidelity of the experimental result $\chi^{(s)}$ is about $\chi^{(s)} = 99.86 \pm 0.01\%$.

With the experimentally determined $\chi$ matrix, we systematically searched for the maximal value for the coherent information $\mathcal{I}_c$. We found that the maximal value of coherence information is about $8.55 \times 10^{-16} \pm 3.50 \times 10^{-16}$ with $\lambda_0 = 0$, $\theta = 7\pi/25$, and $\phi = 47\pi/50$.

Figure 4B shows the coherence information calculated from $\chi^{(s)}$ by scanning $\theta$ and $\lambda_0$ with $\phi$ equal to $47\pi/50$. We can see that the maximal value of coherence information is achieved with $\lambda_0$ equal to 0.

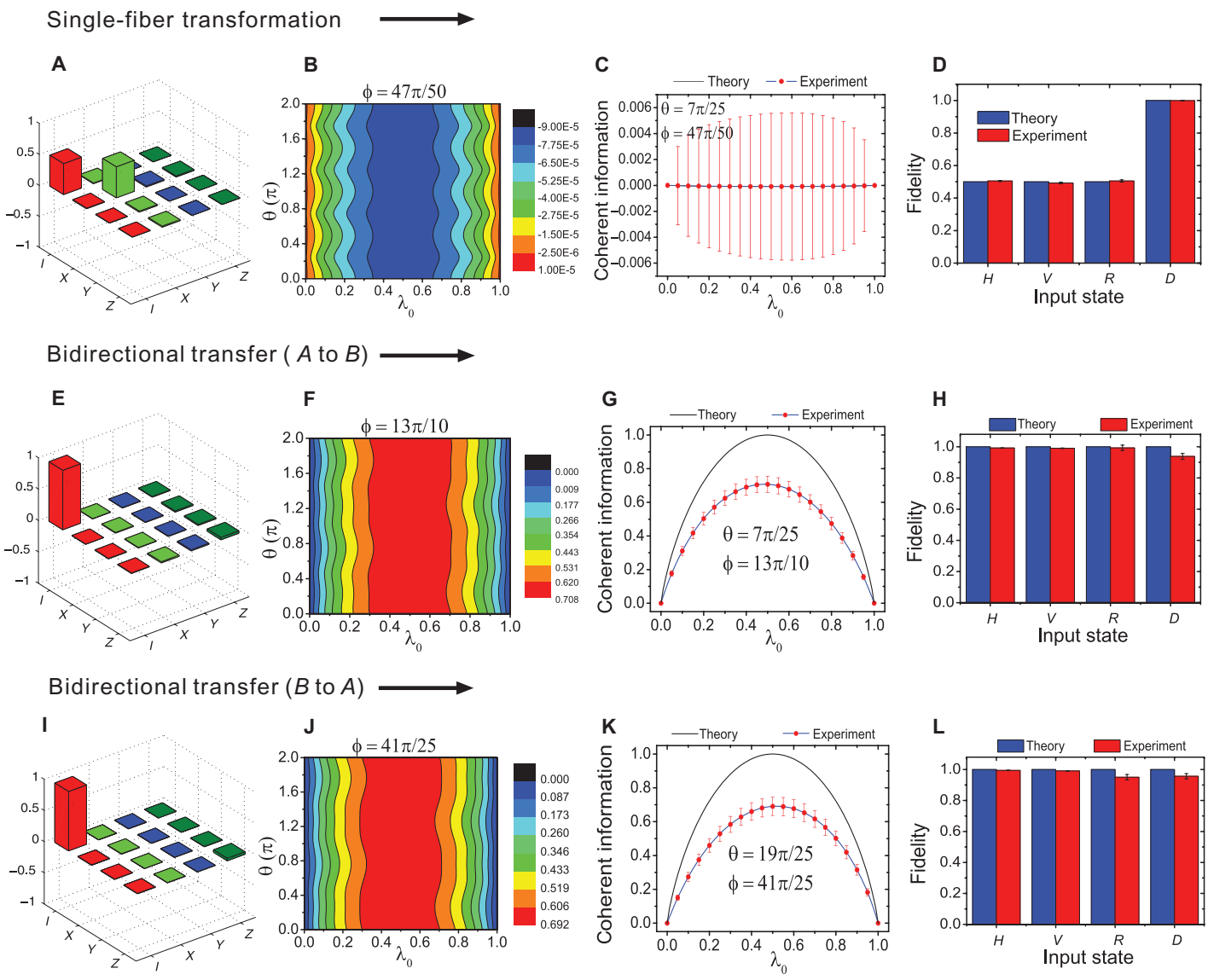


**Fig. 4. Experimental results.** (**A**) The real part of the experimental matrix $\chi^{(s)}$ for a single fiber. (**B**) The coherent information $\mathcal{I}_c$ calculated from $\chi^{(s)}$ by scanning θ and $\lambda_0$, with $\phi = 47\pi/50$. (**C**) Coherent information of the single fiber as a function of $\lambda_0$, with $\theta = 7\pi/25$ and $\phi = 47\pi/50$. The theoretical prediction (black line) agrees with the experimental result (blue line and red dots), which is nearly equal to zero (the black line and the blue line nearly overlap, and only the blue line can be seen). (**D**) The fidelities of different states passing through the single fiber. (**E**) The real part of the experimental mean density matrix $\chi^{(AB)}$ for the bidirectional use from *A* (left) to *B* (right). (**F**) The coherent information calculated from $\chi^{(AB)}$ as a function of θ and $\lambda_0$, with $\phi = 13\pi/10$. (**G**) Coherent information of the paired fibers as a function of $\lambda_0$, with $\theta = 7\pi/25$ and $\phi = 13\pi/10$. The black line represents the theoretical prediction. The blue line and red dots represent the results calculated from $\chi^{(AB)}$ (**H**) The fidelities of different states passing through the paired fibers. (**I**) The real part of the experimental mean density matrix $\chi^{(BA)}$ for the bidirectional use from *B* (right) to *A* (left). (**J**) The coherent information calculated from $\chi^{(BA)}$ as a function of θ and $\lambda_0$, with $\phi = 41\pi/25$. (**K**) Coherent information of the paired fibers as a function of $\lambda_0$ with $\theta = 19\pi/25$ and $\phi = 41\pi/25$. The black line represents the theoretical prediction. The blue line and red dots represent the results calculated from $\chi^{(BA)}$ (**L**) The fidelities of different states passing through the paired fibers. Error bars are estimated from the SD.

The coherence information of the single fiber is further shown as a function of $\lambda_0$ with $\theta = 7\pi/25$ and $\phi = 47\pi/50$ (Fig. 4C). The theoretical prediction (black line) agrees with the experimental result (blue line and red dots), which is nearly equal to zero (the black line and the blue line nearly overlap, and only the blue line can be seen). Error bars are estimated from the SD, and the maximal deviation is about 0.006.

The theoretical (blue columns) and experimental (red columns) fidelities of the four states $\{|H\rangle, |V\rangle, |D\rangle, |R\rangle\}$ are further compared in Fig. 4D. We find that they are in good agreement. Therefore, we conclude that the quantum capacity of the PM fiber is a good approximation to a zero-capacity quantum channel.

## Main experimental results for bidirectional transfer

The experimental data for the bidirectional modes are presented in Fig. 4 (E to H) for quantum information transmitting from left to right (*A* to *B*) in Fig. 2A. Figure 4E shows the real part of the experimental mean

density matrix $\chi^{(AB)}$ (the imaginary part is negligible and is shown in the Supplementary Materials), and the fidelity is calculated to be $\chi^{(AB)}$ = 94.68 ± 0.01%. Figure 4F shows the coherent information calculated from $\chi^{(AB)}$ as a function of θ and $\lambda_0$, with $\phi = 13\pi/10$. Coherent information as a function of $\lambda_0$ with $\theta = 7\pi/25$ and $\phi = 13\pi/10$ is further shown in Fig. 4G. The black line represents the theoretical prediction. The blue line and red dots represent the results calculated from $\chi^{(AB)}$. The fidelities of different states are shown in Fig. 4H.

The experimental data for the bidirectional transfer from *B* to *A* are shown in Fig. 4 (I to L). The real part of the experimental mean density matrix $\chi^{(BA)}$ is shown in Fig. 4I, and the fidelity is calculated to be $\chi^{(BA)}$ = 95.13 ± 0.01%. Figure 4J shows the coherent information calculated from $\chi^{(BA)}$ as a function of θ and $\lambda_0$, with $\phi = 41\pi/25$, and Fig. 4K represents the coherent information as a function of $\lambda_0$, with $\theta = 19\pi/25$ and $\phi = 41\pi/25$. The fidelities of different states are further shown in Fig. 4L. The results clearly show the ability of the setup to bidirectionally transmit quantum information.

### Application to testing quantum nonlocality

Our setup can also be used to transmit nonlocal quantum information. We prepared different kinds of entangled states of the form $|\Psi\rangle = \alpha|HH\rangle + \beta|VV\rangle$ from two type I beta-barium borate (BBO) crystals (*43*), where $\alpha^2$ is set to be {0.1, 0.2, 0.5, 0.8, 0.9}. Our goal is to verify the nonlocality of the output state with maximal entanglement by testing the Clauser-Horne-Shimony-Holt (CHSH) inequality (*44*)

$$S = E(\theta_1, \theta_2) + E(\theta_1, \theta_2') + E(\theta_1', \theta_2) - E(\theta_1', \theta_2') \quad (4)$$

where

$$E(\theta_1, \theta_2) = \frac{c(\theta_1, \theta_2) + c(\theta_1^{\perp}, \theta_2^{\perp}) - c(\theta_1, \theta_2^{\perp} - c(\theta_1^{\perp}, \theta_2))}{c(\theta_1, \theta_2) + c(\theta_1^{\perp}, \theta_2^{\perp}) + c(\theta_1, \theta_2^{\perp} + c(\theta_1^{\perp}, \theta_2))}$$

$\theta_j^{\perp} = \theta_j + 90°$, $j$ = 1, 2, and $c(\theta_1,\theta_2)$ represents the coincidence counts with the polarization angle settings $\theta_1$ in mode *A* and $\theta_2$ in mode *B*.

Figure 5 (A and B) characterizes the properties of the setup for transferring entangled states. Figure 5A shows the corresponding state fidelities when states are transferred from *A* to *B* (cyan columns) and from *B* to *A* (yellow columns). The fidelities of all output states are larger than 90%.

The coherent information with the corresponding input states is further shown in Fig. 5B. The output state $\rho_{A'}$ [$= \mathcal{E}(\rho_A)$] is obtained by tracing photon *B* of the final two-photon state $\rho_{AB'}$ [$= (\mathcal{E} \otimes I)(|\Psi\rangle_{AB}\langle\Psi|)$] to calculate the coherent information. Cyan columns and yellow columns represent the experimental results when states are transferred from *A* to *B* and from *B* to *A*, respectively. We can see that the maximal coherent information is achieved with $\alpha^2 = 0.5$, which agrees with previous results.

Figure 5 (C and D) shows the experimental results of the correlations when states are transferred from *A* to *B* and from *B* to *A*, respectively. The angle settings are calculated from the final density matrixes to maximize the values of *S* ($S \leq 2$ for any local realistic theory). In our experiment, we obtain the values $S = 2.438 \pm 0.025$ in Fig. 5C and $S = 2.542 \pm 0.023$ in Fig. 5D. Both results violate the classical limit well above experimental errors (over about 18 SDs), indicating the incompatibility of local realistic theories.

## DISCUSSION

Our approach can be considered as exploiting a DFS at the single-photon level (that is, without the need for any ancillary photon), but

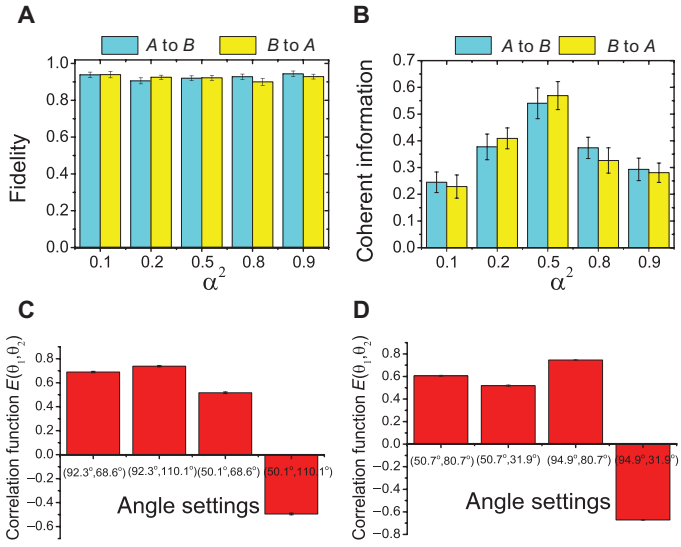


**Fig. 5. Experimental results for the entangled input states with one of the photons passing through the paired PM fibers.** (**A**) The fidelities of the photon states with $\alpha^2$ = 0.1, 0.2, 0.5, 0.8, and 0.9. (**B**) The coherent information with the corresponding input states. (**C** and **D**) The components for obtaining the CHSH values when states are transferred (C) from *A* to *B* ($S = 2.438 \pm 0.025$) and (D) from *B* to *A* ($S = 2.542 \pm 0.023$). Error bars are estimated from the SD.

it is applicable to entangled multiqubit states as well. More precisely, for any given multiqubit state of *n* photons, $|\psi\rangle = \alpha|P\rangle_{n-1}|0\rangle_S + \beta|Q\rangle_{n-1}|1\rangle_S$, where $|P\rangle_{n-1}$ and $|Q\rangle_{n-1}$ are the states of the $n - 1$ qubits entangled with the subsystem photon *S* to be sent through optical fibers.

We note a crucial difference between entanglement distribution and direct quantum state transfer. Both approaches are studied theoretically and experimentally in the literature. Of course, quantum state transfer can be achieved with entanglement distribution in the protocol of quantum teleportation. However, more resources for measurement and feedback control are required to accomplish the task. Here, we focus on direct quantum state transfer (which also covers entangled states) as frequent exchanges of quantum states are expected in generic photonic quantum networks; less operations can potentially lead to a higher efficiency.

Transferring unknown quantum states (from Alice to Bob) using DFS is more challenging than sending known states, like Bell's state $(|01\rangle + |10\rangle)/\sqrt{2}$. The latter case corresponds to the task of entanglement distribution because, for entanglement distribution, one can always reprepare the state if it fails for any probabilistic operation (for example, through a generator located between Alice and Bob).

Furthermore, for quantum state transfer, one may want to transfer only part of a multiqubit state that could come from an intermediate step of some potentially complicated quantum operations; the information encoded in the state would be lost and irrecoverable if it fails. Therefore, state independence is essential for any quantum transmission method for building communication links of a quantum network (Fig. 1).

The time-bin method (*8*) is often exploited to achieve a DFS when two photons are sent through the same optical fiber, when the time delay is sufficiently short that the induced errors are correlated. This approach (*16*, *23*) can be achieved with the use of entangled photons (Fig. 6A), that is, $\alpha|H\rangle + \beta|V\rangle \rightarrow \alpha|H\rangle|V\rangle + \beta|V\rangle|H\rangle$, where $|H\rangle$ and $|V\rangle$ represent the horizontal and vertical polarizations, respectively.

However, currently, the generation of entangled photons remains nondeterministic. The applicability of this approach is therefore limited.

An improvement has been implemented in a series of studies (*21*, *25*, *29*), which relaxed the requirement of entangled input (Fig. 6B). However, this improvement requires the projection to the entangled subspace through a parity-checking operation that can be successful only with a probability of $^1/_2$ (see more details in the Supplementary Materials). The probabilistic operation limits the scalability of this quantum communication protocol for the purpose of building links in a quantum network. For example, sending the state from node 1 to node 2 and then to node 3 will result in the successful probability dropping to $^1/_4$, and so on. This limitation does not exist in our approach.

Furthermore, the time-bin DFS approach typically requires a pair of photons, which are successively sent through the same optical fiber (two photons + one fiber). Our approach provides a more versatile implementation that protects individual photons based on the inference of their paths, that is, a single-photon phenomenon (one photon + two fibers) that acts on individual photons in any multiqubit state. Our construction of DFS for each photon is made possible by the hybrid approach of using both polarization and path DOF; a CNOT gate between them can be achieved deterministically with the use of a PBS. Furthermore, noise correlation in the fibers is maximized through the physical bundling of the paired fibers.

In summary, we have presented a novel scheme that is capable of transmitting quantum information bidirectionally and that avoids many limitations of the existing schemes. Given the currently available technology, the proposed method is mostly suitable for securing short- to medium-distance [for example, $O$(1 to 100) m] quantum communications.

For short- to medium-range applications, there is no significant drawback in our approach to building robust links for photonic quantum information transfer, compared with other existing methods. To extend our method for long-distance transfer (for example, 100 km), we will need to overcome the challenge of stabilizing the relative phase in the interferometer, which can be accomplished easily in our setup (120 m). Furthermore, to increase the error correlation, we bundle the paired fibers together. It is not known how well this technique can be extended for large distances; this problem points to a new research direction. Furthermore, our experimental setting provides a new physical platform for enriching the structure of the quantum channel theory when applied to correlated channels, and the setup has potential application for protecting quantum information in the large-scale photonics implementation of quantum algorithms.

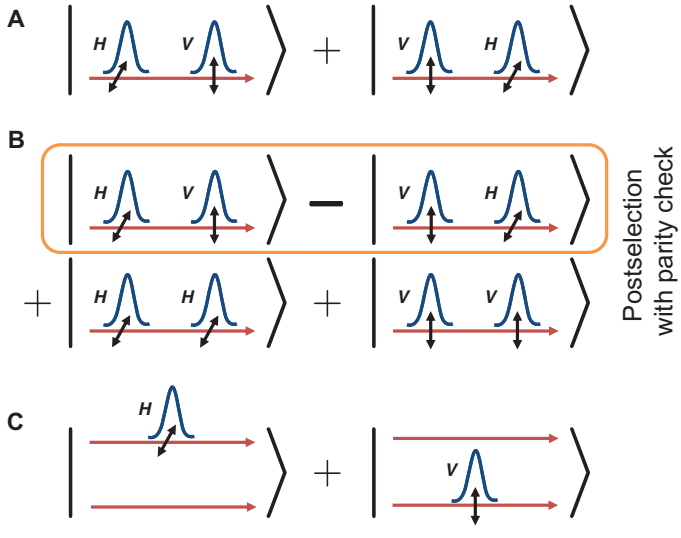


**Fig. 6. Different approaches to constructing DFS for optics.** (**A**) A standard two-photon approach (*16*, *23*) where entangled states are prepared probabilistically. (**B**) An alternative two-photon approach (*21*, *25*, *29*) where the protected subspace is obtained through postselection of a parity check. (**C**) A single-photon approach (applicable for arbitrary multiple-photon states) presented in this report where the path DOF is used to construct an effective DFS.

## MATERIALS AND METHODS

Our experimental setup is shown in Fig. 2. Ultraviolet (UV) pulses were used to pump two type I BBO crystals to produce polarization-entangled photon pairs (*43*). The UV pulses were frequency-doubled from a mode-locked Ti:sapphire laser centered at 800 nm with a 130-fs pulse width and a 76-MHz repetition rate. After compensating for the birefringence effect between $H$ and $V$ in BBO crystals with quartz plates (CP), maximally entangled photon pairs emitted into paths $A$ and $B$. The photon in path $A$ passed through the quantum channel (either a single PM fiber or the encoded paired PM fibers) and was sent to Bob. The photon in path $B$ was triggered into $|H\rangle$, and the photon in path $A$, which was prepared for the corresponding states ($\{|H\rangle, |V\rangle, |D\rangle, |R\rangle\}$), was sent to the interferometer (from left to right) to implement quantum process tomography. To verify bidirectional use, the photon in path $A$ was then triggered into $|H\rangle$, and the photon in path $B$, which was prepared for the corresponding states ($\{|H\rangle, |V\rangle, |D\rangle, |R\rangle\}$), was sent to the interferometer (from right to left) to implement quantum process tomography.

A picosecond pulse laser with a pulse width of about 2.2 ps, a wavelength of 860 nm, and a repetition rate of 76 MHZ was used as a reference light, which was separated from the signal photon by optical gratings at each output port. The reference light was then coupled into a feedback control system by using the piezo motion to lock the relative phase between the two arms of the interferometer (not shown in Fig. 2). Quartz plates were used as compensators to maximize the interference between the two arms.

The polarization of the final state was then analyzed by a quarter-wave plate, an HWP, and a PBS in each arm. The photons were detected by SPADs with 3-nm IFs in front of them.

In our experiment, the counting of each measurement was assumed to follow the Poisson distribution (the subprogram used was PoissonDistribution in Wolfram Mathematica 7.0). We randomly regrouped 50 counting sets for each measurement quantity from the distribution counting. The values of the quantity were calculated from the corresponding counting sets, and 50 values were obtained. The error of the quantity was then estimated by the square root of the variance of the 50 values.

## SUPPLEMENTARY MATERIALS

Supplementary material for this article is available at http://advances.sciencemag.org/cgi/content/full/2/1/e1500672/DC1

Dephasing effect of PM optical fibers

Coherent information

Single-use channel capacity of the completely dephasing channel

Reconstruction of the density matrix $\chi$

## REFERENCES AND NOTES

1. P. Kok, W. J. Munro, K. Nemoto, T. C. Ralph, J. P. Dowling, G. J. Milburn, Linear optical quantum computing with photonic qubits. *Rev. Mod. Phys.* **79**, 135–174 (2007).
2. A. Aspuru-Guzik, P. Walther, Photonic quantum simulators. *Nat. Phys.* **8**, 285–291 (2012).
3. V. Giovannetti, S. Lloyd, L. Maccone, Advances in quantum metrology. *Nat. Photonics* **5**, 222–229 (2011).
4. K. C. Kao, G. A. Hockham, Dielectric-fibre surface waveguides for optical frequencies. *Proc. IEE* **113**, 1151–1158 (1966).
5. A. Kumar, A. Ghatak, *Polarization of Light with Applications in Optical Fibers* (SPIE Press, Bellingham, WA, 2011).
6. P. W. Shor, Scheme for reducing decoherence in quantum computer memory. *Phys. Rev. A* **52**, R2493–R2496 (1995).
7. D. Bacon, Experimental quantum error correction, in Quantum Error Correction, D. A. Lidar, T. A. Brun, Eds. (Cambridge Univ. Press, New York, 2013), pp. 509–518.
8. J. Brendel, N. Gisin, W. Tittel, H. Zbinden, Pulsed energy-time entangled twin-photon source for quantum communication. *Phys. Rev. Lett.* **82**, 2594–2597 (1999).
9. P. G. Kwiat, A. J. Berglund, J. B. Altepeter, A. G. White, Experimental verification of decoherence-free subspaces. *Science* **290**, 498–501 (2000).
10. D. Kielpinski, V. Meyer, M. A. Rowe, C. A. Sackett, W. M. Itano, C. Monroe, D. J. Wineland, A decoherence-free quantum memory using trapped ions. *Science* **291**, 1013–1015 (2001).
11. L. Viola, E. M. Fortunato, M. A. Pravia, E. Knill, R. Laflamme, D. G. Cory, Experimental realization of noiseless subsystems for quantum information processing. *Science* **293**, 2059–2063 (2001).
12. D. A. Lidar, K. B. Whaley, Decoherence-free subspaces and subsystems, in *Irreversible Quantum Dynamics*, F. Benatti, R. Floreanini, Eds. (Springer Lecture Notes in Physics, Springer, Berlin, 2003), pp. 83–120.
13. J. E. Ollerenshaw, D. A. Lidar, L. E. Kay, Magnetic resonance realization of decoherence-free quantum computation. *Phys. Rev. Lett.* **91**, 217904 (2003).
14. M. Mohseni, J. S. Lundeen, K. J. Resch, A. M. Steinberg, Experimental application of decoherence-free subspaces in an optical quantum-computing algorithm. *Phys. Rev. Lett.* **91**, 187903 (2003).
15. Z. D. Walton, A. F. Abouraddy, A. V. Sergienko, B. E. A. Saleh, M. C. Teich, Decoherence-free subspaces in quantum key distribution. *Phys. Rev. Lett.* **91**, 087901 (2003).
16. J.-C. Boileau, R. Laflamme, M. Laforest, C. R. Myers, Robust quantum communication using a polarization-entangled photon pair. *Phys. Rev. Lett.* **93**, 220501 (2004).
17. M. Bourennane, M. Eibl, S. Gaertner, C. Kurtsiefer, A. Cabello, H. Weinfurter, Decoherence-free quantum information processing with four-photon entangled states. *Phys. Rev. Lett.* **92**, 107901 (2004).
18. K. Banaszek, A. Dragan, W. Wasilewski, C. Radzewicz, Experimental demonstration of entanglement-enhanced classical communication over a quantum channel with correlated noise. *Phys. Rev. Lett.* **92**, 257901 (2004).
19. I. Marcikic, H. de Riedmatten, W. Tittel, H. Zbinden, M. Legré, N. Gisin, Distribution of time-bin entangled qubits over 50 km of optical fiber. *Phys. Rev. Lett.* **93**, 180502 (2004).
20. Y.-K. Jiang, X.-B. Wang, B.-S. Shi, A. Tomita, Experimental verification of fault tolerant quantum key distribution protocol. *Opt. Express* **13**, 9415–9421 (2005).
21. T. Yamamoto, J. Shimamura, Ş. K. Özdemir, M. Koashi, N. Imoto, Faithful qubit distribution assisted by one additional qubit against collective noise. *Phys. Rev. Lett.* **95**, 040503 (2005).
22. C. F. Roos, M. Chwalla, K. Kim, M. Riebe, R. Blatt, 'Designer atoms' for quantum metrology. *Nature* **443**, 316–319 (2006).
23. T.-Y. Chen, J. Zhang, J.-C. Boileau, X.-M. Jin, B. Yang, Q. Zhang, T. Yang, R. Laflamme, J.-W. Pan, Experimental quantum communication without a shared reference frame. *Phys. Rev. Lett.* **96**, 150504 (2006).
24. Q. Zhang, J. Yin, T.-Y. Chen, S. Lu, J. Zhang, X.-Q. Li, T. Yang, X.-B. Wang, J.-W. Pan, Experimental fault-tolerant quantum cryptography in a decoherence-free subspace. *Phys. Rev. A* **73**, 020301 (2006).
25. T. Yamamoto, R. Nagase, J. Shimamura, Ş. K. Özdemir, M. Koashi, N. Imoto, Experimental ancilla-assisted qubit transmission against correlated noise using quantum parity checking. *New J. Phys.* **9**, 191 (2007).
26. R. Prevedel, M. S. Tame, A. Stefanov, M. Paternostro, M. S. Kim, A. Zeilinger, Experimental demonstration of decoherence-free one-way information transfer. *Phys. Rev. Lett.* **99**, 250503 (2007).
27. A. D'Arrigo, G. Benenti, G. Falci, Quantum capacity of dephasing channels with memory. *New J. Phys.* **9**, 310 (2007).
28. T. Honjo, S. W. Nam, H. Takesue, Q. Zhang, H. Kamada, Y. Nishida, O. Tadanaga, M. Asobe, B. Baek, R. Hadfield, S. Miki, M. Fujiwara, M. Sasaki, Z. Wang, K. Inoue, Y. Yamamoto, Long-distance entanglement-based quantum key distribution over optical fiber. *Opt. Express* **16**, 19118–19126 (2008).
29. T. Yamamoto, K. Hayashi, Ş. K. Özdemir, M. Koashi, N. Imoto, Robust photonic entanglement distribution by state-independent encoding onto decoherence-free subspace. *Nat. Photonics* **2**, 488–491 (2008).
30. J.-W. Pan, Z.-B. Chen, C.-Y. Lu, H. Weinfurter, A. Zeilinger, M. Żukowski, Multiphoton entanglement and interferometry. *Rev. Mod. Phys.* **84**, 777–838 (2012).
31. T. B. Pittman, B. C. Jacobs, J. D. Franson, Probabilistic quantum logic operations using polarizing beam splitters. *Phys. Rev. A* **64**, 062311 (2001).
32. T. C. Ralph, A. J. F. Hayes, A. Gilchrist, Loss-tolerant optical qubits. *Phys. Rev. Lett.* **95**, 100501 (2005).
33. E. Knill, R. Laflamme, G. J. Milburn, A scheme for efficient quantum computation with linear optics. *Nature* **409**, 46–52 (2001).
34. Here, "unidirectional" means one input from one side and one output at the other side of the communication channel. "Bidirectional" means one input and one output are both located at each side.
35. B. Schumacher, M. A. Nielsen, Quantum data processing and error correction. *Phys. Rev. A* **54**, 2629–2635 (1996).
36. S. Lloyd, Capacity of the noisy quantum channel. *Phys. Rev. A* **55**, 1613–1622 (1997).
37. P. W. Shor, The quantum channel capacity and coherent information, in *Mathematical Science Research Institute Workshop on Quantum Computation* (Berkeley, 2002); http://msri.org/realvideo/ln/msri/2002/quantumcrypto/shor/1/.
38. I. Devetak, The private classical capacity and quantum capacity of a quantum channel. *IEEE Trans. Inf. Theory* **51**, 44–55 (2005).
39. I. Devetak, P. W. Shor, The capacity of a quantum channel for simultaneous transmission of classical and quantum information. *Commun. Math. Phys.* **256**, 287–303 (2005).
40. I. L. Chuang, M. A. Nielsen, Prescription for experimental determination of the dynamics of a quantum black box. *J. Mod. Opt.* **44**, 2455–2467 (1997).
41. J. F. Poyatos, J. I. Cirac, P. Zoller, Complete characterization of a quantum process: The two-bit quantum gate. *Phys. Rev. Lett.* **78**, 390–393 (1997).
42. J. L. O'Brien, G. J. Pryde, A. Gilchrist, D. F. V. James, N. K. Langford, T. C. Ralph, A. G. White, Quantum process tomography of a controlled-NOT gate. *Phys. Rev. Lett.* **93**, 080502 (2004).
43. P. G. Kwiat, E. Waks, A. G. White, I. Appelbaum, P. H. Eberhard, Ultrabright source of polarization-entangled photons. *Phys. Rev. A* **60**, R773–R776 (1999).
44. J. F. Clauser, M. A. Horne, A. Shimony, R. A. Holt, Proposed experiment of test local hidden-variable theories. *Phys. Rev. Lett.* **23**, 880–884 (1969).

**Acknowledgments:** We thank Y. Ouyang, J. Fitzsimons, and K. Li for valuable comments and suggestions. **Funding:** This work was supported by the National Basic Research Program of China (grant no. 2011CB921200), the National Natural Science Foundation of China (grant nos. 11274297, 11004185, 61322506, 60921091, 11274289, 11325419, and 61327901), the Fundamental Research Funds for the Central Universities (grant nos. WK2470000011 and WK2470000020), the Program for New Century Excellent Talents in University (NCET-12-0508), the Science Foundation for Excellent PhD Thesis (grant no. 201218), and the Youth Innovation Promotion Association and Excellent Young Scientist Program, Chinese Academy of Sciences. M.-H.Y. was supported by the National Basic Research Program of China (grant nos. 2011CBA00300 and 2011CBA00301) and the National Natural Science Foundation of China (grant nos. 61033001, 11405093, and 61361136003). **Author contributions:** J.-S.X. and C.-F.L. designed the experiment. M.-H.Y. provided the theoretical analysis. J.-S.X. performed the experiment with the assistance of X.-Y.X. and J.-S.T. C.-F.L. and G.-C.G. supervised the project. M.-H.Y. and J.-S.X. wrote the paper. All authors discussed the experimental results. **Competing interests:** The authors declare that they have no competing interests. **Data and materials availability:** All data needed to evaluate the conclusions in the paper are present in the paper and/or the Supplementary Materials. Additional data related to this paper may be requested from the authors.

Submitted 25 May 2015
Accepted 7 September 2015
Published 8 January 2016
10.1126/sciadv.1500672

**Citation:** J.-S. Xu, M.-H. Yung, X.-Y. Xu, J.-S. Tang, C.-F. Li, G.-C. Guo, Robust bidirectional links for photonic quantum networks. *Sci. Adv.* **2**, e1500672 (2016).

Science Advances

# Robust bidirectional links for photonic quantum networks

Jin-Shi Xu, Man-Hong Yung, Xiao-Ye Xu, Jian-Shun Tang, Chuan-Feng Li and Guang-Can Guo

*Sci Adv* **2** (1), e1500672.
DOI: 10.1126/sciadv.1500672



*Science Advances* (ISSN 2375-2548) is published by the American Association for the Advancement of Science, 1200 New York Avenue NW, Washington, DC 20005. 